***Title*: Ataxia Telangiectasia Mutated coordinates the ovarian DNA repair and atresia-initiating response to phosphoramide mustard**

Kendra L. Clark and Aileen F. Keating*

Department of Animal Science – Iowa State University, Ames, Iowa 50011

*Running title*: *Atm* haploinsufficiency impacts the DNA damage response

*Summary sentence:* DNA repair is coordinated by ovarian ATM

*Keywords:* DNA repair, ovary, ovotoxicity, oncofertility

*Corresponding author: Aileen F. Keating, 2356H Kildee Hall, Department of Animal Science, Iowa State University, Ames, Iowa 50011, Email: akeating@iastate.edu

This work was in part funded by the Bailey Career Development Award from Iowa State University (AFK).

*Disclosure statement:* The authors have nothing to disclose.

**Abstract**

Ataxia telangiectasia mutated (ATM) protein recognizes and repairs DNA double strand breaks (DSB) through activation of cell cycle checkpoints and DNA repair proteins. *Atm* gene mutations increase female reproductive cancer risk. Phosphoramide mustard (PM) induces ovarian DNA damage and destroys primordial follicles, and pharmacological ATM inhibition prevents PM-induced follicular depletion. Wild-type (WT) C57BL/6 or $Atm^{+/-}$ mice were dosed once intraperitoneally with sesame oil (95%) or PM (25 mg/kg) in the proestrus phase of the estrous cycle and ovaries harvested 3 days thereafter. $Atm^{+/-}$ mice spent ~25% more time in diestrus phase than WT. LC-MS/MS on ovarian protein was performed and bioinformatically analyzed. Relative to WT, $Atm^{+/-}$ mice had 64 and 243 proteins increased or decreased in abundance, respectively. In WT mice, PM increased 162 and decreased 20 proteins. In $Atm^{+/-}$ mice, 173 and 37 proteins were increased and decreased, respectively, by PM. Exportin-2 (XPO2) was localized to granulosa cells of all follicle stages and was 7.2-fold greater in $Atm^{+/-}$ than WT mice. Cytoplasmic FMR1-interacting protein 1 (CYFIP1) was 6.8-fold lower in $Atm^{+/-}$ mice and was located in the surface epithelium with apparent translocation to the ovarian medulla post-PM exposure. PM induced γH2AX, but fewer γH2AX positive foci were identified in $Atm^{+/-}$ ovaries. Similarly, cleaved caspase-3 was lower in the $Atm^{+/-}$ PM-treated, relative to WT mice. These findings support ATM involvement in ovarian DNA repair and suggest that ATM functions to regulate ovarian atresia.

## Introduction

The integrity of the genome is constantly insulted by endogenous and exogenous sources and an intrinsic response is needed to effectively repair any damaged DNA. Ataxia telangiectasia mutated (ATM) protein is a major orchestrator of DNA repair and activated ATM precipitates the cellular DNA damage repair response (DDR). The cell cycle is arrested, and the DNA damage is fixed, or the cell is triggered for apoptosis if beyond repair [1]. ATM acts as a sensor and transducer of DNA damage, phosphorylating several downstream targets after activation including histone 2AX (H2AX) [2], mediator of DNA damage checkpoint protein 1 (MDC1) [3], and breast cancer type 1 susceptibility protein (BRCA1) [4] for DNA repair; serine/threonine-protein kinase Chk2 (CHK2) for cell cycle arrest [5]. After the repair process, ATM influences cellular fate by targeting p53 [6] for apoptosis, and RAC-alpha serine/threonine-protein kinase (AKT) [7] for cell survival. Elevated ATM is associated with a poor tumor response to chemotherapy and platinum resistance [8].

Mutations in *Atm* cause ataxia-telangiectasia (A-T) syndrome, a rare autosomal recessive disease characterized by neurodegeneration, immunodeficiency, increased radiosensitivity, cancer predisposition, and infertility [9]. A-T women have hypoplastic ovaries devoid of primordial follicles [10] and female $Atm^{-/-}$ mice are infertile and lack viable oocytes [11]. Women who are heterozygous carriers of mutated *Atm* have elevated cancer risk, particularly breast and ovarian [12-17], thus, receive anti-cancer therapy; a scenario that further increases their infertility risks.

Cyclophosphamide (CPA) is an alkylating agent used in the treatment of cancers [18] and autoimmune disorders [19, 20] in adults and children. Phosphoramide mustard (PM), an

ovotoxic metabolite of CPA [21, 22], destroys rapidly dividing cells by inducing DNA double strand breaks (DSB) [23]. The reproductive effects of PM exposure have been well characterized by our group and others, which include loss of primordial and primary follicles in mice [24-27], antral follicles in rats [28], and amenorrhea, premature ovarian failure, and infertility in women and young girls [29]. In addition to fertility issues, CPA exposure has been associated with congenital malformations in offspring exposed to CPA *in ute*ro as well as pre-gestational germ cell exposures [30]. Increasing cancer survival rates present the need to identify the mechanisms by which cancer therapies or other chemical exposures cause ovarian damage.

ATM induction is the earliest observed event during PM-induced ovotoxicity and our group made the surprising observation that pharmacological inhibition of ATM prevents PM-induced follicular depletion *ex vivo* [31]. Thus, the hypothesis under investigation in this study was that the DNA damage response would be blunted in $Atm^{+/-}$ deficient mice and unhealthy follicles that normally would be triggered for repair and/or apoptosis would remain in the ovary. Our specific objectives were to determine if lowered ATM abundance affected PM-induced follicle loss and to investigate abundance and localization of ovarian DNA repair and apoptosis proteins after PM exposure in both wild type and ATM-deficient mice.

## Materials and Methods

### Animal procedure and tissue collection

All experiments were performed according to regulatory guidelines and approved by the Institutional Animal Care and Use Committee (IACUC) and Institutional Biosafety Committee at Iowa State University. Female C57BL/6J (n = 6) and B6.129S6-$Atm^{tm1Awb}$/J mice (referred to as

*Atm*$^{+/-}$ herein; n = 6) were purchased from Jackson Laboratory (Bar Harbor, ME) and maintained in an animal facility at Iowa State University under controlled room temperature (21°C-22°C) and lighting (12hr light:12hr dark) with *ad libitum* access to food and water. At 10 weeks of age, mice were intraperitoneally (IP) injected once with PM (25 mg/kg) or sesame oil (95%; n = 3 per group) in the pro-estrus phase of the estrous cycle. Mice were euthanized 3 days after dosing at which time body and organ weights were recorded. Organ weights were normalized to body weight. Ovaries were collected and one ovary was fixed in 4% paraformaldehyde overnight at 4°C for histological analysis while the contralateral ovary was snap frozen in liquid nitrogen and stored at -80°C until processing for protein extraction.

**Estrous Cycle Monitoring**

The estrous cycle was monitored by performing vaginal cytology analysis in the morning for 10 days to ensure that mice were at the same stage of the estrous cycle for PM dosing. Briefly, fresh, wet vaginal smears were collected by pipetting saline into the vagina and collecting the samples. Vaginal smears were placed onto histology slides and examined with a Nikon OPTIPHOT microscope using a 10X objective. Classification of estrous cycle stages was determined as previously described [32]. During the follicular phase, pro-estrus was characterized by small, round nucleated epithelial cells, some cornified epithelial cells, and little to no leukocytes. Estrus was characterized by several cornified epithelial cells containing deteriorating nuclei. The presence of cornified cells and leukocytes indicated the metestrus stage. In diestrus, nucleated epithelial cells reappeared in the vaginal smears in addition to the presence of polymorphonuclear leukocytes.

**Histology and Follicle Counting**

After fixation, ovaries were passed through a 10%, 20%/0.1M PBS gradient for 1-3 hours each at room temperature, followed by 30% sucrose/0.1M PBS overnight at 4°C and embedded in optimal cutting temperature (OCT) compound before being flash frozen on dry ice. Serial sections were cut at 7 μm on a cryostat (Leica CM1850) and every 6$^{th}$ section was mounted onto glass slides and stained with hematoxylin and eosin for follicle counting, while intermittent sections were retained for immunofluorescence staining. Healthy follicles containing oocytes with a distinct oocyte nucleus were counted and classified as previously described [33]. Briefly, primordial follicles were identified by an oocyte encircled by a single layer of squamous granulosa cells; primary follicles contained an oocyte surrounded by a single layer of cuboidal granulosa cells; secondary follicles contained an oocyte surrounded by multiple layers of granulosa cells, and antral follicles were identified as those containing an oocyte enclosed by several layers of granulosa cells in conjunction with presence of a fluid filled antral space. Follicle counts and bright field images were captured on an inverted DMI3000B microscope (Leica) and QICAM MicroPublisher 5.0 (MP5.0-RTV-CLR-10, QIMAGING) camera using QCapture software at a 5x objective. Total counted follicle numbers per ovary were compared between treatments.

**Protein Isolation and Proteome Analysis**

Total ovarian protein was isolated by tissue homogenization in lysis buffer (50 mM Tris-HCL, 1 mM EDTA, pH 8.5) followed by centrifugation at 10,000 rpm at 4°C for 15 min. Supernatant was collected and protein content was quantified using a bicinchoninic acid assay (BCA) and prepared as a working dilution (50 μg/uL) with lysis buffer (Pierce BCA Protein

Assay Kit, Thermofisher). Protein (50 µg/µl) was digested with trypsin/Lys-C for 16 hours, dried down and reconstituted in buffer A (47.5µl; 0.1% formic acid/water). Peptide Retention Time Calibration (PRTC) mixture (25 fmol/µl) was spiked into each sample as an internal control. Protein (10 µg) and PRTC (250 fmol) were injected onto a liquid chromatography column (Agilent Zorbax SB-C18, 0.5mm x 150mm, 5 micron) using an Agilent 1260 Infinity Capillary Pump. Peptides were separated by liquid chromatography and analyzed using a Q Exactive™ Hybrid Quadrupole-Orbitrap Mass Spectrometer with an HCD fragmentation cell. A positive identification was considered only if three positive peptides were identified per protein. The resulting intact and fragmentation pattern was compared to a theoretical fragmentation pattern (from either MASCOT or Sequest HT) to identify peptides. The relative abundance of the identified proteins was based on the areas of the top three unique peptides for each sample.

For each peptide, the signal intensity was divided by the arithmetic mean of the PRTC as the normalization factor before further analysis. MetaboAnalyst 4.0 [34] was used for data analysis. Upon finding data integrity to be satisfactory (no peptide with more than 50% missing replicates, positive values for the area), missing value estimation was imputed using Singular Value Decomposition (SVD) method. Non-informative values that were near-constant throughout the experiment conditions were detected using interquartile range (IQR) estimation method and were deleted. Data transformation was performed based on generalized logarithm transformation (glog) to make individual features more comparable. The control and treatment samples were compared by *t*-test with the adjusted *P*-value (FDR) cutoff of 0.05. Fold change (FC) analysis with threshold of 2 was performed to compare the absolute value of change between control and treatment values. A volcano plot was created to combine the FC and the *t*-test analysis. The PCA analysis was performed using the *prccomp* package and pairwise score

plots were created to provide an overview of the various separation patterns among the most significant components. Partial least squared (PLS*)* regression was then performed using the *plsr* function provided by R *pls* package to predict the continuous and discrete variables. A PLS-DA model was built to classify and cross-validate PLS using the *caret* package. Finally, a dendrogram and a Heatmap were generated to graphically represent the data.

The UniProt protein IDs that were up/down regulated with *P*-values less than 0.05 were used to retrieve the corresponding KEGG IDs using the "Retrieve/ID mapping" tool of UniProt (accessible at http://www.uniprot.org/uploadlists/). KEGG IDs were used to retrieve biological pathway association of the proteins. Enrichment analysis was performed using the Database for Annotation, Visualization and Integrated Discovery (DAVID) 6.8 Tools [35].

**Gene Ontology Analysis**

Gene Ontology (GO) analysis was performed using PANTHER version 14.0 (http://www.pantherdb.org). Proteins identified in the control and experimental samples were compared to the *Mus musculus* reference list and divided into protein class and biological process. The Fisher's Exact test with False Discovery Rate (FDR) correction was used with $P < 0.05$ considered as a significant difference between samples.

**Immunofluorescence staining**

Slides were warmed briefly on a 37°C slide warmer and tissue sections were encircled with a histology pap pen (Vector Laboratories) to keep staining solutions concentrated on the tissue during processing. Tissue was rehydrated and permeabilized in 0.1M PBS with 0.1% Tween20 (PBSTw) for 20 min, followed by serum blocking (0.1M PBS/1% BSA/1% DMSO/5%

goat serum) for 60 min at room temperature. Primary antibodies (**Supplemental Table 1**) were diluted in fresh blocking solution and applied to the tissue sections and incubated in a humidified box at 4°C overnight. For antigen retrieval, 1% sodium dodecyl sulfate (SDS) was applied for 5 min after rehydration, followed by three washes of PBSTw for 5 min each and addition of blocking solution as described above. After primary antibody incubation, slides were washed 6 times in PBSTw for 5 min per wash. The appropriate secondary antibody (**Supplemental Table 1**) was added to fresh blocking solution, applied to tissue sections and incubated at room temperature for 60 min, followed by 6 washes in PBSTw for 5 min per wash. Slides were air dried, followed by addition of Vectashield with DAPI (H1200, Vector Labs) and cured overnight at 4°C. Negative technical controls to confirm specificity were performed using secondary antibodies alone (**Supplemental Figure 1**). Images were captured on a Zeiss LSM700 confocal microscope equipped with an AxioCam MRc5 using a 5 or 20x objective.

**Quantification of Protein Abundance**

For quantification of BRCA1, H2AX, and cytochrome c (CYCS) immunoreactivity (n = 3 ovaries per treatment; 2 sections per ovary), the threshold percentage of the total ovarian image area was analyzed in whole ovarian sections using ImageJ (https://imagej.nih.gov). When quantifying ATM immunoreactivity, the threshold percentage of the total image area was limited to the oocyte (3 ovaries per treatment; 17-35 oocytes per treatment), while XPO2 immunoreactivity was measured in granulosa cells of antral follicles (3 ovaries per treatment; 18-45 follicles per treatment). For γH2AX (3 ovaries per treatment; 30-39 follicles per treatment) and cleaved CASP3 (3 ovaries per treatment; 33-36 follicles per treatment), immunopositive

cells were manually counted in primary, secondary and antral follicles using the cell counter module of ImageJ (https://imagej.nih.gov/ij/plugins/cell-counter.html).



**Statistical Analysis**

Statistical analyses were performed using GraphPad Prism 7.0 two-way ANOVA function with Tukey multiple comparison tests for follicle numbers, organ weights, and immunofluorescent staining values. The unpaired t-test was used in the evaluation of the estrous cycle and body weights. For the estrous cycle data, the statistical analysis was performed on the raw data and the data is presented as percentage of time spent at that stage of the estrous cycle during the monitoring period. Bars represent mean value ± standard error of the mean (SEM). A *P*-value ≤ 0.05 was considered statistically significant and a trend for a statistical difference was considered at $P < 0.1$.

**Results**

**Effect of phosphoramide mustard exposure on body and organ weight**

Body weight was lower in $Atm^{+/-}$ females relative to WT controls ($P < 0.05$; **Supplemental Figure 2**) at the onset of the experiment. There was no effect of either PM exposure or *Atm* deficiency on weight of the heart, kidney, liver, spleen, uterus or ovary ($P > 0.05$; **Supplemental Figure 2**).

**Impact of *Atm* deficiency on estrous cyclicity and follicle number**

There was no impact of *Atm* deficiency on the length of time spent in the proestrus, metestrus, or estrus phases of the estrous cycle; however, $Atm^{+/-}$ mice remained in the diestrus phase of the estrous cycle longer than their WT counterparts ($P < 0.05$; **Figure 1D**). There were

reduced numbers of primordial ($P < 0.05$), primary ($P < 0.1$), and total ($P < 0.05$) number of follicles in ovaries of *Atm*$^{+/-}$ mice relative to WT controls (**Figure 2E-G**) but no impact of *Atm* deficiency on secondary or antral follicle number (data not shown).

**Effect of PM exposure on follicle number**

Phosphoramide mustard decreased ($P < 0.05$) the number of healthy primordial follicles in WT ovaries by 77% (**Figure 2E**). However, comparison between the *Atm*$^{+/-}$ mice who received vehicle control and the *Atm*$^{+/-}$ mice who received PM, revealed no effect ($P > 0.05$) of PM exposure on primordial follicle number in *Atm*$^{+/-}$ ovaries, though the number of primordial follicles was reduced by 52% (**Figure 2E**). Phosphoramide mustard decreased the number of healthy primary follicles in the WT ovaries by 37%, but similar to primordial follicle numbers, relative to *Atm*$^{+/-}$ mice who received vehicle control, PM did not reduce primary follicle number in *Atm*$^{+/-}$ mice (**Figure 2F**). PM exposure also did not affect the number of healthy secondary or antral follicles in WT or *Atm*$^{+/-}$ mice (data not shown). Total follicle number was less in both the CT and PM-exposed *Atm*$^{+/-}$ mice and in WT PM-exposed relative to the WT CT mice (**Figure 2G**). There was no PM-induced difference in total follicle number in *Atm*$^{+/-}$ mice (**Figure 2G**). Overall, there was a reduction in 51% of all follicle types in WT ovaries due to PM treatment, with only a 36% decline in all follicles observed in the *Atm*$^{+/-}$ ovaries.

**Identification of PM-induced DNA damage and protein markers of ATM-mediated double strand break repair**

To determine an altered ovarian DDR and/or atresia in *Atm*$^{+/-}$ ovaries, protein markers of DNA damage and the DDR were examined. Positive ATM immunofluorescent staining was

observed in the oocyte in all follicle stages, with no difference in localization pattern between genotypes or treatment (**Figure 3A**). ATM immunoreactivity decreased in intensity between the PM-treated genotypes ($P < 0.05$), but no other differences were noted (**Figure 3A'**).

To determine if *Atm*$^{+/-}$ mice have increased amounts of DNA damage basally and to assess the DDR after a genotoxic exposure, the abundance of ovarian γH2AX was investigated and positive γH2AX foci were quantified in all follicular stages (**Figure 3B**). Increased positive γH2AX foci were detected in WT ovaries after PM-treatment ($P < 0.05$; **Figure 3B'**). In the *Atm*$^{+/-}$ ovaries, PM exposure did not increase γH2AX (**Figure 3B'**). There was no effect of genotype or PM treatment on the abundance of non-phosphorylated H2AX (**Supplemental Figure 3A**).

BRCA1 immunofluorescent staining was observed throughout the ovary in the oocytes of primary, secondary, and antral follicles, theca cells, stromal cells, with moderate staining occuring in the granulosa cells of some antral follicles (**Figure 3C** and **Supplemental Figure 3B**). Whole ovary BRCA1 fluorescence intensity was decreased in PM-treated WT ovaries, relative to the WT controls (**Figure 3C'**). There was lower BRCA1 protein staining in the vehicle control-treated *Atm*$^{+/-}$ ovaries compared to the corresponding WT controls ($P < 0.05$; **Figure 3C'**). PM exposure in *Atm*$^{+/-}$ mice did not impact BRCA1 protein abundance as detected by immunofluorescent staining (**Figure 3C'**).

Granulosa cells that stained positively for cleaved CASP3 were assessed by immunological staining and positive cells quantified in all follicular stages (**Figure 4A**). An increase in CASP3 positive cells in the WT ovaries after PM-treatment ($P < 0.05$) was observed, and this was absent in *Atm*$^{+/-}$ PM-treated ovaries, relative to the corresponding control. Reduced

($P < 0.1$) numbers of cleaved CASP3 cells were observed in *Atm*$^{+/-}$ PM-treated, relative to WT PM exposed ovaries (**Figure 4A'**).

CYCS protein abundance was determined by immunofluorescent staining and was observed throughout the entire ovary. Lack of ATM did not impact basal CYCS, nor was an impact of PM exposure on ovarian CYCS in WT mice observed (**Figure 4B**). There was a trend ($P < 0.1$) for reduced CYCS in *Atm*$^{+/-}$ovaries exposed to PM (**Figure 4B'**).

**Proteomic alterations due to *Atm* haploinsufficiency**

LC-MS/MS was utilized to determine any proteins of interest that are regulated by ATM. There were 2,123 ovarian proteins identified in vehicle control-treated *Atm*$^{+/-}$ mice and 2,145 ovarian proteins identified in the vehicle control WT mice. Relative to the WT vehicle control-treated ovaries, 64 proteins were increased and 243 were decreased in abundance in the ovaries of *Atm*$^{+/-}$ females ($P \leq 0.05$; **Supplemental Table 2**).

**Effect of phosphoramide mustard exposure on the ovarian proteome**

In addition to determining proteins regulated by ATM, LC-MS/MS analysis determined those altered by PM treatment. A total of 2,160 proteins were identified in PM-exposed WT ovaries. Relative to the WT controls, 162 proteins were increased, and 20 proteins were reduced in ovaries of WT mice exposed to PM ($P \leq 0.05$; **Supplemental Table 3**). In PM-treated *Atm*$^{+/-}$ mice, 2,132 proteins were identified, and 173 proteins were increased and 37 decreased compared to *Atm*$^{+/-}$ mice treated with vehicle control ($P \leq 0.05$; **Supplemental Table 4**). In *Atm*$^{+/-}$ mice exposed to PM, 116 proteins were decreased and 61 increased ($P \leq 0.05$; **Supplemental Table 5**) compared to WT PM-exposed mice.

Of these differentially expressed proteins that were increased in each PM treated group, 132, 141, and 31 were determined to be unique in WT, *Atm*$^{+/-}$, and in the PM-treated genotype comparison, respectively (**Figure 5A**). In contrast, 20, 37, and 116 proteins were decreased that were exclusive to the PM-treated WT, *Atm*$^{+/-}$, and genotype comparisons, accordingly (**Figure 5B**). Within the separate genotypes and in the absence of PM treatment, 39 increased proteins were identified as unique (**Figure 5A**), while 243 proteins were identified as decreased (**Figure 5B**). Additionally, there were 58 shared proteins that were increased between all groups and 49 proteins shared that were decreased between all groups (**Figure 5A-B)**. 49 proteins were shared between the genotypes, with 16 of these proteins being upregulated and 33 downregulated (**Figure 5A-B**).

*Gene ontology (GO) and pathway analysis*

Differentially abundant proteins between *Atm*$^{+/-}$ and WT mice were assigned to protein class and biological process using PANTHER GO analysis (Fischer's Exact with FDR multiple test correction; $P < 0.05$). GO analysis distributed 221 hit genes into 21 protein classes for proteins identified as differing in the *Atm*$^{+/-}$ vehicle control relative to the WT vehicle control (**Figure 5C-D**). In the *Atm*$^{+/-}$ PM relative to WT PM, 139 hit genes were distributed into 22 protein classes (**Figure 5C-D**). Most of the proteins identified were classified as nucleic acid binding proteins (28% in vehicle control-treated ovaries, 15% in PM-treated ovaries; **Figure 5C-D**). Protein classes with the greatest assignments were hydrolases, transferases, enzyme modulators, and cytoskeletal proteins. Together, these protein classes comprise of ~65% of proteins identified between the WT and *Atm*$^{+/-}$ vehicle-treated mice and ~58% of those proteins identified in the WT and *Atm*$^{+/-}$ PM-exposed mice.

For biological process, 43 proteins from the control exposure groups and 27 proteins from the PM exposure groups were assigned to the cellular metabolic process cluster, representing around 15% of the proteins over-represented in *Atm*$^{+/-}$ ovaries. Protein-containing complex subunit organization, establishment of cellular localization, and intracellular transport also had several proteins assigned (**Supplemental Figure 4A**).

KEGG ID's were identified via the UniProt ID mapping tool and utilized in a pathway enrichment analysis via DAVID to determine the representation of molecular networks in *Atm*$^{+/-}$ relative to WT ovaries. In PM exposed mice, the metabolic pathways ID was enriched in approximately ~18% of proteins (**Supplemental Figure 4B**). Interestingly, this was not observed in vehicle control-treated mice of either genotype. Other KEGG pathways identified as differing between the genotypes regardless of treatment were spliceosome, ribosome, focal adhesion, and proteoglycans in cancer (**Supplemental Figure 4B**).

**Effect of PM exposure on ovarian localization of CYFIP1 and XPO2 in WT and *Atm*$^{+/-}$ mice.**

To determine the spatio-temporal distribution of proteins of interest identified in the LC-MS/MS analysis, immunofluorescence staining was performed on whole ovarian sections. In the LC-MS/MS analysis, Cytoplasmic FMR1-interacting protein 1 (CYFIP1) was reduced by 6.83-fold and 5.57-fold in *Atm*$^{+/-}$ vehicle-control and *Atm*$^{+/-}$ PM exposed ovaries, respectively, relative to their wild-type counterparts. CYFIP1 positive cells were uniformly spaced along the ovarian surface epithelium in all ovary samples (**Figure 6A** and **6A'**), however, PM exposure altered this localization and post-PM exposure, CYFIP1 protein was present in the ovarian cortex including granulosa cells and medulla (**Figure 6A** and **6A'**).

Exportin-2 (XPO2) increased in the *Atm*$^{+/-}$ vehicle-control compared to the WT vehicle-control ovaries by 7.20-fold and by 6.40-fold in *Atm*$^{+/-}$ PM-exposed ovaries relative to the WT PM-exposed ovaries as detected by LC-MS/MS analysis. XPO2 immunological staining revealed positive staining in the granulosa cells of all follicular stages and the oocyte, as well as in the corpus luteum (**Figure 6B**).

## Discussion

Cells employ a highly conserved pathway to sense, signal, and repair DNA. A key event in DNA repair is activation of ATM, a member of the phosphatidylinositol 3-kinase (PI3K) superfamily, which also includes ataxia telangiectasia and Rad3-related (ATR) and DNA-dependent protein kinase (DNA-PK) [1]. ATM is activated by the MRN complex, which contains MRE11, RAD50, and NBS1 proteins [36], initiating serine 1981 autophosphorylation and homodimer to active monomer dissociation [37, 38]. Over 700 ATM and ATR protein targets have been identified [39], including BRCA1 [4], CHK2 [5], and P53 [6].

The exact mechanisms underlying chemotherapy-induced follicle loss remain unclear. Direct toxicity to the follicle or oocyte may occur [40-43] or accelerated hyperactivation of primordial follicles [44] in response to targeted death of larger growing follicles, resulting in follicular “burnout” [45-47]. PM induces ovarian DNA damage in the oocyte and granulosa cells [22, 24, 25] and our group discovered that ATM inhibition prevents PM-induced follicle depletion [31]. To further explore the events post-genotoxicant induced ovarian damage, both targeted and exploratory approaches were utilized to determine mechanisms involved in the ovarian response to PM exposure and further, *Atm*$^{+/-}$ mice were employed to interrogate the role of ATM in mediating the PM-induced ovarian response.

In response to PM exposure in WT mice, both primordial and small primary follicle numbers were reduced in WT mice, consistent with our previous findings [26, 27]. Different numbers of growing follicles post-PM treatment were not observed, suggesting lack of hyperactivation of the ovarian reserve. This corresponded with our previous findings in which inhibition of PI3K did not have any effect on the extent of PM-induced follicle loss [48]. The *Atm*$^{+/-}$ mice had reduced follicle number at all stages of development, highlighting the importance of ATM in basal ovarian physiology and recapitulating phenotypic observations in A-T female patients [9]. *Atm*$^{-/-}$ female mice [49] and female A-T patients [9] are infertile due to reduced or complete absence of gametes in the ovary. Primordial germ cell migration to the genital ridge is unaffected in *Atm*$^{-/-}$ mice, but oocytes undergo apoptotic degeneration prior to birth [11]. Adult *Atm*$^{-/-}$ mouse ovaries are also devoid of oocytes and superovulation is ineffective [49].

Similar to our findings in which ATM was pharmacologically inhibited ATM in *ex vivo* cultured ovaries [31], PM-induced follicle loss was less robust in *Atm*$^{+/-}$ mice, relative to WT mice. The effect was not complete inhibition of PM-induced follicle loss, presumably due to *Atm* haploinsufficiency, rather than complete ATM reduction as observed in the pharmacological approach [31]. The level of basal ATM in *Atm*$^{+/-}$ ovaries did not differ relative to WT, but there was lack of increased ATM after PM exposure, supporting lack of ATM responsiveness to PM exposure in these mice.

Upon DNA damage, ATM phosphorylates H2AX to γH2AX at the DNA DSB site, resulting in a positive feedback loop of DNA repair proteins [51-55] and γH2AX presence is considered the gold standard for DSB localization [56]. The DDR was irregular, as evidenced by fewer γH2AX positive cells, in *Atm*$^{+/-}$ mice post-PM treatment. This was in stark contrast with

WT PM mice in which there was accumulation of γH2AX positive cells. This observation was not attributable to reduced total H2AX protein abundance in the *Atm*$^{+/-}$ mice. The numerical lesser abundance of inactive H2AX could be related to reduced ATM, as the two proteins are products of their respective genes, *Atm* and *H2ax*, which are very closely linked in the same cytogenetic region (11q23) in both humans and mice [57].

BRCA1 functions in homologous recombination [58, 59] and nonhomologous end joining DNA repair [60, 61] and is phosphorylated by ATM. Similar to carriers of a mutant *Atm* gene, women with *Brca1* mutations have defective DNA repair and increased risks of breast and ovarian cancers [64]. Relative to ovaries from WT vehicle-control mice, there were lower levels of basal BRCA1 protein in *Atm*$^{+/-}$ vehicle-control ovaries, and in PM-exposed mice (both WT and *Atm*$^{+/-}$), potentially an indication that BRCA1 is depleted in response to PM exposure as a reflection of BRCA1 function though this remains to be determined. Taken together, these findings suggest that ovarian BRCA1 is a direct ATM target and that PM exposure affects ovarian BRCA1.

When DNA damage exceeds the capacity of the cell for repair, it is shunted towards apoptosis. Pro-apoptotic CASP3 is implicated in granulosa [65] and luteal [66] cell death, though not necessary for oocyte death [65]. Despite a dramatic increase in CASP3 positive cells in the WT mice post-PM exposure, fewer cells positively stained for CASP3 in *Atm*$^{+/-}$ female mice after PM exposure. This finding in the WT mice is consistent with previous studies [21, 25, 43, 67]. DNA damage can also activate the mitochondrial apoptosis pathway and CYCS release [68]. Altered CYCS abundance was not noted in this study, though there was a slight decline in CYCS due to PM exposure in the *Atm*$^{+/-}$ ovaries which was not apparent in the WT ovaries. An association between *Atm* deficiency and mitochondrial dysfunction has been documented [70-

72]. Thus, these findings support reduced apoptosis in the *Atm*$^{+/-}$ ovaries in response to PM induction, potentially indicating lack of shunting of damaged follicles towards atresia, as supported by the reduced extent of follicle loss that resulted from PM exposure in the *Atm*$^{+/-}$ mice.

To complement the targeted approach focused on the ovarian DDR and apoptotic proteins, an unbiased proteomic LC-MS/MS approach was employed to determine additional proteins of interest regulated by ATM and altered by PM. The top proteins affected in each comparison are described below, though this does not indicate that proteins that are significantly altered but with a lowered fold-change have lesser importance in the influence of ATM on ovarian function or in the response to PM exposure. KEGG identifiers from our proteome analysis revealed proteins involved in metabolic pathways including pyridoxine 5'-phosphate oxidase (PNPO) and phosphomannomutase 2 (PMM2), and proteins associated with the spliceosome.

Identification of proteins that are increased when ATM functionality is reduced support that they are proteins regulated by ATM or that experience secondary effects upon ATM loss. RPL29 is associated with ovarian cancer malignancy [79]. ME is involved in the luteal transition [80]. NID1 functions in ovarian steroidogenesis and bisphenol A exposure reduced *Nid1* mRNA in Sertoli cells of mice [81, 82].

Lack of appropriate ATM function resulted in reduced abundance of proteins that have been demonstrated to respond to cellular stress. AHSA1 is regulated by p53 and though roles in the ovary are not understood, AHSA increases PI3K phosphorylation [83] thus suggesting involvement in ovarian processes of importance. PMM2 mutations result in a glycosylation disorder in humans and endoplasmic reticulum stress has been reported in a zebrafish model of

PMM2 deficiency [84, 85]. *Nalp14* mRNA transcript is located in the oocytes of follicles up until the preovulatory stage [86] and *Nalp14* mutation is associated with spermatogenic issues in men [87]. Though not well explored, NESP2 was found to be highly expressed in the ovary [88] and NESP1 [89] and NESP3 [90] have roles in the testes supporting a gonadal role for ovarian NESP2.

Identification of proteins increased in response to PM exposure support their involvement in the ovarian protective response (OPR). These findings identify potential targets that could be medicinally induced in the ovary during CPA/PM treatment to minimize ovarian damage that occurs as a treatment side effect. BHMT1 is involved in metabolism of homocysteine which can be regulated in the oocyte via this enzyme [91]. Though the ovarian role is not clear, in the testes, ALD1 is found in the vas deferens and regulated by dihydrotestosterone (DHT) [93]. *Idi1* mRNA is present in reproductive tissue of *Aedes aegypti* mosquito [94], though there is little data on function in mammalian reproductive systems. CP51A is a member of the cytochrome P450 enzyme family of proteins, which are critical in chemical metabolism processes [95]. In the testis, CP51A has an important role in the production of sterols that regulate meiosis [96]. CDN1B or p27kip1 regulates ovarian development in mice through suppression of follicle endowment, activation, and promoting cell death [97].

The proteins that are reduced by PM could represent targets that are used as a mode of action of PM to induce ovotoxicity or could indicate that the abundance of these proteins is reduced due to their being depleted as they are being utilized in the OPR to PM exposure. PDS5B regulates the cohesion of sister chromatids during mitosis and meiosis, a function integral to DNA replication and repair [98]. In males, PDS5B regulates androgen-induced proliferation inactivation [99] and loss of PDS5B has been implicated in prostate cancer [100].

A10A9 has been identified in fluid of ovarian carcinomas and in the serum from ovarian carcinoma patients [101]. DDX18 is a member of the DEAD-box helicase family of proteins [102] and though there is no known specific reproductive tissue roles of DDX18, DDX25 is a gonadotropin-regulated testicular helicase and is essential for spermatogenesis [103]. Increased TPS1 is observed during follicular atresia in primate ovaries [104] and inhibits VEGF, suggesting a role for TSP1 as a mediator for ovarian angiogenesis and follicle development [105]. Little is known about CE162 in reproductive tissues.

In ovaries with reduced basal ATM, ovarian proteins that are responsive to PM exposure were identified, potentially indicating a response that is not solely due to the genotoxic effects of PM. In addition, considering the importance of maintaining gamete quality, there are likely ATM-independent mechanisms to respond to genotoxicants, and these proteins may be part of that response. KINH maintains chromosomal stability and in mouse oocytes is critical for germinal vesicle breakdown and polar body extrusion [106]. NAL14 is an inflammosome component and *Nlrp14* has been detected in mammalian oocytes [107, 108]. In ovarian cancer stem cells, SYQ/QARS binds to aggregated P53 protein [109]. CNN1 is a tumor suppressor with suppressive effects in ovarian cancer cells [110] and is also observed in Sertoli cells [111], as a marker for peritubular myoid cells which interact with Sertoli cells during seminiferous tubule development [112]. Conversely, ILK has been implicated in pro-metastatic epithelial ovarian cancers [113].

As is the case with the proteins that are increased in response to PM when ATM is deficient, the same is true of those proteins that are reduced in abundance. These reductions could represent utilization of these proteins in the response to PM, and could also indicate that with decreased abundance of ATM, proteins for which no apparent alteration in their overall

abundance during PM exposure in the WT ovaries could in fact be functional in that scenario, but then be reduced in ovarian content in ATM deficiency, and that they are depleted at a faster rate or to a greater extent when ATM is insufficient. MGRAP is a mitochondrial transmembrane protein in the ovary (previously named ovary specific acidic protein) [114, 115] and *Mgrap* is regulated by estrogen and suppressed by a GnRH antagonist [118]. MBD2 has been identified in breast cancer cells [119]. AIF1L was identified via microarray as upregulated in ovarian cancer tissue versus normal ovarian tissue [120]. Reduced HMGN5 increases chemosensitivity of human bladder cancer cells through inhibition of PI3K/AKT signaling [121], but it also has an oncogenic role in several types of cancers including breast [122] and prostate [123]. AFAM has been detected in follicular fluid [124], with serum concentrations remaining stable throughout the menstrual cycle [125] and elevated in polycystic ovary syndrome patients [126].

Two proteins chosen for further characterization to decipher the impact of PM exposure in the ovaries of the WT and $Atm^{+/-}$ mice were CYFIP and XPO2. CYFIP1 was dramatically decreased in ovaries from $Atm^{+/-}$ female mice both basally and in response to PM treatment relative to their wild-type counterparts. *Cyfip1* is frequently deleted or reduced in human epithelial cancers and during invasion of epithelial tumors, with silencing of *Cyfip1* resulting in disorganized epithelial morphogenesis *in vitro* [127]. Our finding of alterations to CYFIP1 in the $Atm^{+/-}$ ovary with localization around the ovarian surface epithelium and the appearance of CYFIP1 positive cells within the ovarian cortex and medulla after PM treatment indicates a possible role of CYFIP1 in ovarian tissue architecture, notable considering the increased rates of ovarian cancers in A-T female patients as well as carriers of a mutated *Atm* allele.

The cellular apoptosis susceptibility protein XPO2 (also known as CSE1L) was greatly increased in the $Atm^{+/-}$ female ovary both due to ATM deficiency and post-PM exposure in

contrast to WT ovaries in which this response was not observed. In healthy cells, the function of XPO2 has been proposed as a breakpoint in regulating which cells proliferate and which cells undergo apoptosis [130]. Modifications in abundance of *Xpo2* have been suggested to promote neoplasia in breast cancers [131-134]. Furthermore, increased *Xpo2* in association with the tumor suppressor gene *Bax* and pro-apoptotic *Casp3*, coincide with reduced anti-apoptotic *Bcl-2* has been demonstrated in the pathogenesis of endometrial carcinomas [135]. Considering that PM induced ovarian apoptosis in WT, but not in $Atm^{+/-}$ mice, these data suggest that XPO2 may be involved in ATM-mediated apoptosis.

In addition to implications for effective DNA repair, *Atm* haploinsufficiency may impact ovarian aging. BRCA1 mutation carriers undergo earlier menopause, suggestive of decreased ovarian reserve [73-76]. Similarly, DNA repair gene and protein activity in the ovary decreases with age [76, 77] illustrating the relationship between DNA DSB repair and ovarian aging. The $Atm^{+/-}$ females spent ~25% more time in the diestrus phase of the estrous cycle. Further, the reduced follicle numbers in the absence of PM exposure supports our observation of altered estrous cycles in the $Atm^{+/-}$ females, indicative of POF. When reproductive aging begins, the disorganization of the estrous cycle is characterized by cycles with varying lengths and declining fertility [78]. These results suggest that carriers of the *Atm* mutation may experience earlier menopause onset in addition to subfecundity.

In conclusion, these findings identify proteins involved in the ovarian response to the genotoxicant, PM. This study also underscores the importance of ATM protein to the ability of the ovary to mount the OPR to a genotoxicant. Further, proteins that may be involved in an ATM-independent ovarian response to a DNA damaging insult have been identified, which could lead to therapeutic targets to improve fertility in females who undergo anti-cancer

treatments. In addition, the data herein provides strong support for a role of ATM in regulating how follicles that retain DNA damage are shunted towards an atretic demise, further highlighting the importance of ATM in multiple roles in coordination of the OPR. These findings are of importance to women undergoing cancer treatment for whom lessening the ovotoxicity side effects are of paramount importance. The information reported herein also has value for *Atm*$^{+/-}$ human carriers and women who experience idiopathic POF. Finally, these data add to the basic understanding of the OPR that is mounted to maintain germline integrity and ovarian function.

**Figure Legends**

**Figure 1. Impact of *Atm* deficiency on estrous cyclicity.** The percentage time spent in proestrus (**A**), estrus (**B**), metestrus (**C**), diestrus (**D**) phase of the estrous cycle was calculated based upon vaginal cytological assessments in wildtype (WT) and *Atm*$^{+/-}$ mice. Difference from WT is indicated by * = $P < 0.05$.

**Figure 2. *Atm* deficiency reduces follicle number and alters PM-induced ovotoxicity.** Representative hematoxylin and eosin stained ovarian sections from (**A**) WT CT; (**B**) WT PM; (**C**) *Atm*$^{+/-}$ CT; or (**D**) *Atm*$^{+/-}$ PM are presented; scale bar = 200 μm. Follicles were classified as (**E**) primordial; (**F**) primary; (**G**) total and counted. Bars represent mean follicle number ± SEM. Difference between treatments is indicated by the # = $P < 0.1$, * = $P < 0.05$.

**Figure 3. Effect of *Atm* deficiency and PM exposure on DNA damage proteins**. Primary antibodies directed against (**A**) ATM, (**B**) γH2AX, and (**C**) BRCA1 were used to determine ovarian localization in WT CT; WT PM; *Atm*$^{+/-}$ CT; and *Atm*$^{+/-}$ PM mice. Green staining

indicates the protein of interest while DNA is stained in blue; scale bar = 50 μm (20x magnification (0.5x-1x zoom). Double tailed arrow indicates theca cells; dotted tail arrow indicates granulosa cells; O indicates oocyte. Quantification of mean fluorescence intensity and/or immunopositive foci ± SEM for (**A'**) ATM; (**B'**) γH2AX; (**C'**) BRCA1. Difference between treatments is indicated by * = $P < 0.05$.

**Figure 4. Effect of *Atm* deficiency and PM exposure on cell death proteins**. Primary antibodies directed against (**A**) CASP3, and (**B**) CYCS were used to determine ovarian localization in WT CT; WT PM; $Atm^{+/-}$ CT; and $Atm^{+/-}$ PM. Green staining indicates the protein of interest while DNA is stained in blue; scale bar = 50 μm (20x magnification (0.5x-1x zoom). Dotted tail arrow indicates granulosa cells; O indicates oocyte. Quantification of fluorescence intensity and/or immunopositive foci ± SEM for (**A'**) CASP3; and (**B'**) CYCS. Difference between treatments is indicated by # = $P < 0.1$, * = $P < 0.05$.

**Figure 5. Global proteomic effects of *Atm* deficiency and PM exposure.** The Venn diagram presents the number of ovarian proteins identified as being unique to genotype/treatment or altered in common by genotype/treatment. (**A**) Proteins identified as increased; (**B**) Proteins identified as decreased. The number in the orange oval indicates the number of proteins identified in the $Atm^{+/-}$ CT as being different from the WT CT group; the blue oval indicates the number of proteins identified in the WT PM group as being different from the WT CT; the green oval indicates the number of proteins in the $Atm^{+/-}$ PM group that differ from the $Atm^{+/-}$ CT; and the red oval indicates the number of proteins in the $Atm^{+/-}$ PM group that differ from the WT PM. Overlapping areas of the circles illustrate the number of proteins that were altered by two or

more groups. Distribution of the proteins identified in (**C**) *Atm*$^{+/-}$/WT CT and (**D**) *Atm*$^{+/-}$/WT PM according to PANTHER protein class.

**Figure 6. Ovarian localization of CYFIP1 and XPO2.** The ovarian location of CYFIP1 and XPO2 proteins were assessed by immunofluoresence staining. (**A**) CYFIP1 (5x magnification); (**A'**) CYFIP1 (20x magnification); (**B**) XPO2 protein were localized in the ovary of WT CT; WT PM; *Atm*$^{+/-}$ CT; and *Atm*$^{+/-}$ PM mice. Green staining indicates the protein of interest while DNA is stained in blue; 5x magnification scale bar = 200 μm, 20x scale bar = 50 μm. Dotted tail arrow indicates granulosa cells; solid arrow indicates ovarian surface epithelium; white box indicates area imaged for 20x magnification; blue dotted circle indicates ovarian medulla.

References


1. Savitsky, K., et al., *A single ataxia telangiectasia gene with a product similar to PI-3 kinase.* Science, 1995. **268**(5218): p. 1749-53.
2. Rogakou, E.P., et al., *Megabase chromatin domains involved in DNA double-strand breaks in vivo.* J Cell Biol, 1999. **146**(5): p. 905-16.
3. Lou, Z., et al., *MDC1 maintains genomic stability by participating in the amplification of ATM-dependent DNA damage signals.* Mol Cell, 2006. **21**(2): p. 187-200.
4. Gatei, M., et al., *Role for ATM in DNA damage-induced phosphorylation of BRCA1.* Cancer Res, 2000. **60**(12): p. 3299-304.
5. Falck, J., et al., *The ATM-Chk2-Cdc25A checkpoint pathway guards against radioresistant DNA synthesis.* Nature, 2001. **410**(6830): p. 842-7.

6. Meulmeester, E., et al., *ATM-mediated phosphorylations inhibit Mdmx/Mdm2 stabilization by HAUSP in favor of p53 activation.* Cell Cycle, 2005. **4**(9): p. 1166-70.
7. Liu, Q., et al., *Role of AKT signaling in DNA repair and clinical response to cancer therapy.* Neuro Oncol, 2014. **16**(10): p. 1313-23.
8. Abdel-Fatah, T.M., et al., *ATM, ATR and DNA-PKcs expressions correlate to adverse clinical outcomes in epithelial ovarian cancers.* BBA Clin, 2014. **2**: p. 10-7.
9. Boder, E. and R.P. Sedgwick, *Ataxia-telangiectasia; a familial syndrome of progressive cerebellar ataxia, oculocutaneous telangiectasia and frequent pulmonary infection.* Pediatrics, 1958. **21**(4): p. 526-54.
10. Fortuno, C. and E. Labarta, *Genetics of primary ovarian insufficiency: a review.* J Assist Reprod Genet, 2014. **31**(12): p. 1573-85.
11. Barlow, C., et al., *Atm deficiency results in severe meiotic disruption as early as leptonema of prophase I.* Development, 1998. **125**(20): p. 4007-17.
12. Su, Y. and M. Swift, *Mortality rates among carriers of ataxia-telangiectasia mutant alleles.* Ann Intern Med, 2000. **133**(10): p. 770-8.
13. Swift, M., et al., *Incidence of cancer in 161 families affected by ataxia-telangiectasia.* N Engl J Med, 1991. **325**(26): p. 1831-6.
14. Swift, M., et al., *Breast and other cancers in families with ataxia-telangiectasia.* N Engl J Med, 1987. **316**(21): p. 1289-94.
15. Inskip, H.M., et al., *Risk of breast cancer and other cancers in heterozygotes for ataxia-telangiectasia.* Br J Cancer, 1999. **79**(7-8): p. 1304-7.
16. Janin, N., et al., *Breast cancer risk in ataxia telangiectasia (AT) heterozygotes: haplotype study in French AT families.* Br J Cancer, 1999. **80**(7): p. 1042-5.
17. Olsen, J.H., et al., *Cancer in patients with ataxia-telangiectasia and in their relatives in the nordic countries.* J Natl Cancer Inst, 2001. **93**(2): p. 121-7.
18. Colvin, O.M., *An overview of cyclophosphamide development and clinical applications.* Curr Pharm Des, 1999. **5**(8): p. 555-60.
19. Henderson, L., et al., *Treatment for lupus nephritis.* Cochrane Database Syst Rev, 2012. **12**: p. Cd002922.
20. Suarez-Almazor, M.E., et al., *Cyclophosphamide for rheumatoid arthritis.* Cochrane Database Syst Rev, 2000(2): p. Cd001157.
21. Plowchalk, D.R. and D.R. Mattison, *Phosphoramide mustard is responsible for the ovarian toxicity of cyclophosphamide.* Toxicol Appl Pharmacol, 1991. **107**(3): p. 472-81.
22. Desmeules, P. and P.J. Devine, *Characterizing the ovotoxicity of cyclophosphamide metabolites on cultured mouse ovaries.* Toxicol Sci, 2006. **90**(2): p. 500-9.
23. Surya, Y.A., J.M. Rosenfeld, and B.L. Hillcoat, *Cross-linking of DNA in L1210 cells and nuclei treated with cyclophosphamide and phosphoramide mustard.* Cancer Treat Rep, 1978. **62**(1): p. 23-9.
24. Petrillo, S.K., et al., *Detection of DNA damage in oocytes of small ovarian follicles following phosphoramide mustard exposures of cultured rodent ovaries in vitro.* Toxicol Appl Pharmacol, 2011. **253**(2): p. 94-102.
25. Ganesan, S. and A.F. Keating, *Phosphoramide mustard exposure induces DNA adduct formation and the DNA damage repair response in rat ovarian granulosa cells.* Toxicol Appl Pharmacol, 2015. **282**(3): p. 252-8.

26. Ganesan, S., et al., *Obesity alters phosphoramide mustard-induced ovarian DNA repair in mice.* Biol Reprod, 2017. **96**(2): p. 491-501.
27. Madden, J.A. and A.F. Keating, *Ovarian xenobiotic biotransformation enzymes are altered during phosphoramide mustard-induced ovotoxicity.* Toxicol Sci, 2014. **141**(2): p. 441-52.
28. Ataya, K.M., E.F. Pydyn, and A.J. Ramahi-Ataya, *The effect of "activated" cyclophosphamide on human and rat ovarian granulosa cells in vitro.* Reprod Toxicol, 1990. **4**(2): p. 121-5.
29. Meirow, D., *Reproduction post-chemotherapy in young cancer patients.* Mol Cell Endocrinol, 2000. **169**(1-2): p. 123-31.
30. Rengasamy, P., *Congenital Malformations Attributed to Prenatal Exposure to Cyclophosphamide.* Anticancer Agents Med Chem, 2017. **17**(9): p. 1211-1227.
31. Ganesan, S. and A.F. Keating, *The ovarian DNA damage repair response is induced prior to phosphoramide mustard-induced follicle depletion, and ataxia telangiectasia mutated inhibition prevents PM-induced follicle depletion.* Toxicol Appl Pharmacol, 2016. **292**: p. 65-74.
32. Byers, S.L., et al., *Mouse estrous cycle identification tool and images.* PLoS One, 2012. **7**(4): p. e35538.
33. Pedersen, T. and H. Peters, *Proposal for a classification of oocytes and follicles in the mouse ovary.* J Reprod Fertil, 1968. **17**(3): p. 555-7.
34. Chong, J., et al., *MetaboAnalyst 4.0: towards more transparent and integrative metabolomics analysis.* Nucleic Acids Res, 2018. **46**(W1): p. W486-w494.
35. Huang da, W., B.T. Sherman, and R.A. Lempicki, *Systematic and integrative analysis of large gene lists using DAVID bioinformatics resources.* Nat Protoc, 2009. **4**(1): p. 44-57.
36. Uziel, T., et al., *Requirement of the MRN complex for ATM activation by DNA damage.* Embo j, 2003. **22**(20): p. 5612-21.
37. Bakkenist, C.J. and M.B. Kastan, *DNA damage activates ATM through intermolecular autophosphorylation and dimer dissociation.* Nature, 2003. **421**(6922): p. 499-506.
38. Kozlov, S., et al., *ATP activates ataxia-telangiectasia mutated (ATM) in vitro. Importance of autophosphorylation.* J Biol Chem, 2003. **278**(11): p. 9309-17.
39. Matsuoka, S., et al., *ATM and ATR substrate analysis reveals extensive protein networks responsive to DNA damage.* Science, 2007. **316**(5828): p. 1160-6.
40. Perez, G.I., X.J. Tao, and J.L. Tilly, *Fragmentation and death (a.k.a. apoptosis) of ovulated oocytes.* Mol Hum Reprod, 1999. **5**(5): p. 414-20.
41. Kerr, J.B., et al., *Cisplatin-induced primordial follicle oocyte killing and loss of fertility are not prevented by imatinib.* Nat Med, 2012. **18**(8): p. 1170-2; author reply 1172-4.
42. Kim, S.Y., et al., *Transient inhibition of p53 homologs protects ovarian function from two distinct apoptotic pathways triggered by anticancer therapies.* Cell Death Differ, 2019. **26**(3): p. 502-515.
43. Luan, Y., et al., *Inhibitors of apoptosis protect the ovarian reserve from cyclophosphamide.* J Endocrinol, 2019. **240**(2): p. 243-256.
44. Keating, A.F., et al., *Effect of phosphatidylinositol-3 kinase inhibition on ovotoxicity caused by 4-vinylcyclohexene diepoxide and 7, 12-dimethylbenz[a]anthracene in neonatal rat ovaries.* Toxicol Appl Pharmacol, 2009. **241**(2): p. 127-34.

45. Kalich-Philosoph, L., et al., *Cyclophosphamide triggers follicle activation and "burnout"; AS101 prevents follicle loss and preserves fertility.* Sci Transl Med, 2013. **5**(185): p. 185ra62.
46. Chang, E.M., et al., *Cisplatin Induces Overactivation of the Dormant Primordial Follicle through PTEN/AKT/FOXO3a Pathway which Leads to Loss of Ovarian Reserve in Mice.* PLoS One, 2015. **10**(12): p. e0144245.
47. Morgan, S., et al., *Cisplatin and doxorubicin induce distinct mechanisms of ovarian follicle loss; imatinib provides selective protection only against cisplatin.* PLoS One, 2013. **8**(7): p. e70117.
48. Madden, J.A., P.Q. Thomas, and A.F. Keating, *Phosphoramide mustard induces autophagy markers and mTOR inhibition prevents follicle loss due to phosphoramide mustard exposure.* Reprod Toxicol, 2017. **67**: p. 65-78.
49. Barlow, C., et al., *Atm-deficient mice: a paradigm of ataxia telangiectasia.* Cell, 1996. **86**(1): p. 159-71.
50. Zenzes, M.T., *Smoking and reproduction: gene damage to human gametes and embryos.* Hum Reprod Update, 2000. **6**(2): p. 122-31.
51. Paull, T.T., et al., *A critical role for histone H2AX in recruitment of repair factors to nuclear foci after DNA damage.* Curr Biol, 2000. **10**(15): p. 886-95.
52. Stucki, M. and S.P. Jackson, *gammaH2AX and MDC1: anchoring the DNA-damage-response machinery to broken chromosomes.* DNA Repair (Amst), 2006. **5**(5): p. 534-43.
53. Kobayashi, J., et al., *NBS1 localizes to gamma-H2AX foci through interaction with the FHA/BRCT domain.* Curr Biol, 2002. **12**(21): p. 1846-51.
54. Ward, I.M., et al., *Accumulation of checkpoint protein 53BP1 at DNA breaks involves its binding to phosphorylated histone H2AX.* J Biol Chem, 2003. **278**(22): p. 19579-82.
55. Kouzarides, T., *Chromatin modifications and their function.* Cell, 2007. **128**(4): p. 693-705.
56. Fernandez-Capetillo, O., et al., *H2AX: the histone guardian of the genome.* DNA Repair (Amst), 2004. **3**(8-9): p. 959-67.
57. Monni, O. and S. Knuutila, *11q deletions in hematological malignancies.* Leuk Lymphoma, 2001. **40**(3-4): p. 259-66.
58. Scully, R., et al., *Association of BRCA1 with Rad51 in mitotic and meiotic cells.* Cell, 1997. **88**(2): p. 265-75.
59. Moynahan, M.E., et al., *Brca1 controls homology-directed DNA repair.* Mol Cell, 1999. **4**(4): p. 511-8.
60. Wang, H., et al., *Nonhomologous end-joining of ionizing radiation-induced DNA double-stranded breaks in human tumor cells deficient in BRCA1 or BRCA2.* Cancer Res, 2001. **61**(1): p. 270-7.
61. Baldeyron, C., et al., *A single mutated BRCA1 allele leads to impaired fidelity of double strand break end-joining.* Oncogene, 2002. **21**(9): p. 1401-10.
62. Cortez, D., et al., *Requirement of ATM-dependent phosphorylation of brca1 in the DNA damage response to double-strand breaks.* Science, 1999. **286**(5442): p. 1162-6.
63. Cousineau, I., C. Abaji, and A. Belmaaza, *BRCA1 regulates RAD51 function in response to DNA damage and suppresses spontaneous sister chromatid replication slippage:*

*implications for sister chromatid cohesion, genome stability, and carcinogenesis.* Cancer Res, 2005. **65**(24): p. 11384-91.
64. Robson, M., et al., *BRCA-associated breast cancer in young women.* J Clin Oncol, 1998. **16**(5): p. 1642-9.
65. Matikainen, T., et al., *Caspase-3 gene knockout defines cell lineage specificity for programmed cell death signaling in the ovary.* Endocrinology, 2001. **142**(6): p. 2468-80.
66. Carambula, S.F., et al., *Caspase-3 is a pivotal mediator of apoptosis during regression of the ovarian corpus luteum.* Endocrinology, 2002. **143**(4): p. 1495-501.
67. Nguyen, Q.N., et al., *Loss of PUMA protects the ovarian reserve during DNA-damaging chemotherapy and preserves fertility.* Cell Death Dis, 2018. **9**(6): p. 618.
68. Igosheva, N., et al., *Maternal diet-induced obesity alters mitochondrial activity and redox status in mouse oocytes and zygotes.* PLoS One, 2010. **5**(4): p. e10074.
69. Martin, S.J. and D.R. Green, *Protease activation during apoptosis: death by a thousand cuts?* Cell, 1995. **82**(3): p. 349-52.
70. Patel, A.Y., et al., *Ataxia telangiectasia mutated influences cytochrome c oxidase activity.* Biochem Biophys Res Commun, 2011. **405**(4): p. 599-603.
71. Ambrose, M., J.V. Goldstine, and R.A. Gatti, *Intrinsic mitochondrial dysfunction in ATM-deficient lymphoblastoid cells.* Hum Mol Genet, 2007. **16**(18): p. 2154-64.
72. Mercer, J.R., et al., *DNA damage links mitochondrial dysfunction to atherosclerosis and the metabolic syndrome.* Circ Res, 2010. **107**(8): p. 1021-31.
73. Rzepka-Gorska, I., et al., *Premature menopause in patients with BRCA1 gene mutation.* Breast Cancer Res Treat, 2006. **100**(1): p. 59-63.
74. Finch, A., et al., *Frequency of premature menopause in women who carry a BRCA1 or BRCA2 mutation.* Fertil Steril, 2013. **99**(6): p. 1724-8.
75. Lin, W.T., et al., *Comparison of age at natural menopause in BRCA1/2 mutation carriers with a non-clinic-based sample of women in northern California.* Cancer, 2013. **119**(9): p. 1652-9.
76. Titus, S., et al., *Impairment of BRCA1-related DNA double-strand break repair leads to ovarian aging in mice and humans.* Sci Transl Med, 2013. **5**(172): p. 172ra21.
77. Govindaraj, V., R. Keralapura Basavaraju, and A.J. Rao, *Changes in the expression of DNA double strand break repair genes in primordial follicles from immature and aged rats.* Reprod Biomed Online, 2015. **30**(3): p. 303-10.
78. Lerner, S.P., et al., *Age-related alterations in follicular development and hormonal profiles in rats with 4-day estrous cycles.* Biol Reprod, 1990. **42**(4): p. 633-8.
79. Li, Y.L., et al., *Identification of suitable reference genes for gene expression studies of human serous ovarian cancer by real-time polymerase chain reaction.* Anal Biochem, 2009. **394**(1): p. 110-6.
80. Klinken, S.P. and P.M. Stevenson, *Changes in enzyme activities during the artificially stimulated transition from follicular to luteal cell types in rat ovary.* Eur J Biochem, 1977. **81**(2): p. 327-32.
81. Tainaka, H., et al., *Evaluation of the testicular toxicity of prenatal exposure to bisphenol A based on microarray analysis combined with MeSH annotation.* J Toxicol Sci, 2012. **37**(3): p. 539-48.

82. Irving-Rodgers, H.F., et al., *Studies of granulosa cell maturation in dominant and subordinate bovine follicles: novel extracellular matrix focimatrix is co-ordinately regulated with cholesterol side-chain cleavage CYP11A1.* Reproduction, 2009. **137**(5): p. 825-34.
83. Okayama, S., et al., *p53 protein regulates Hsp90 ATPase activity and thereby Wnt signaling by modulating Aha1 expression.* J Biol Chem, 2014. **289**(10): p. 6513-25.
84. Mukaigasa, K., et al., *Nrf2 activation attenuates genetic endoplasmic reticulum stress induced by a mutation in the phosphomannomutase 2 gene in zebrafish.* Proc Natl Acad Sci U S A, 2018. **115**(11): p. 2758-2763.
85. Bortot, B., et al., *PMM2-CDG: phenotype and genotype in four affected family members.* Gene, 2013. **531**(2): p. 506-9.
86. Horikawa, M., et al., *The mouse germ-cell-specific leucine-rich repeat protein NALP14: a member of the NACHT nucleoside triphosphatase family.* Biol Reprod, 2005. **72**(4): p. 879-89.
87. Westerveld, G.H., et al., *Mutations in the testis-specific NALP14 gene in men suffering from spermatogenic failure.* Hum Reprod, 2006. **21**(12): p. 3178-84.
88. Lam le, T., et al., *Nesprin-2 epsilon: a novel nesprin isoform expressed in human ovary and Ntera-2 cells.* Biochem Biophys Res Commun, 2011. **412**(2): p. 291-5.
89. Gob, E., et al., *Mammalian sperm head formation involves different polarization of two novel LINC complexes.* PLoS One, 2010. **5**(8): p. e12072.
90. Ketema, M., et al., *Nesprin-3 connects plectin and vimentin to the nuclear envelope of Sertoli cells but is not required for Sertoli cell function in spermatogenesis.* Mol Biol Cell, 2013. **24**(15): p. 2454-66.
91. Benkhalifa, M., et al., *Imprinting: RNA expression for homocysteine recycling in the human oocyte.* Fertil Steril, 2010. **93**(5): p. 1585-90.
92. Schaefer, C.B., et al., *Epigenetic decisions in mammalian germ cells.* Science, 2007. **316**(5823): p. 398-9.
93. Dassouli, A., et al., *Vas deferens epithelial cells in subculture: a model to study androgen regulation of gene expression.* J Mol Endocrinol, 1995. **15**(2): p. 129-41.
94. Diaz, M.E., et al., *Characterization of an isopentenyl diphosphate isomerase involved in the juvenile hormone pathway in Aedes aegypti.* Insect Biochem Mol Biol, 2012. **42**(10): p. 751-7.
95. Foti, R.S. and D.K. Dalvie, *Cytochrome P450 and Non-Cytochrome P450 Oxidative Metabolism: Contributions to the Pharmacokinetics, Safety, and Efficacy of Xenobiotics.* Drug Metab Dispos, 2016. **44**(8): p. 1229-45.
96. Debeljak, N., M. Fink, and D. Rozman, *Many facets of mammalian lanosterol 14alpha-demethylase from the evolutionarily conserved cytochrome P450 family CYP51.* Arch Biochem Biophys, 2003. **409**(1): p. 159-71.
97. Rajareddy, S., et al., *p27kip1 (cyclin-dependent kinase inhibitor 1B) controls ovarian development by suppressing follicle endowment and activation and promoting follicle atresia in mice.* Mol Endocrinol, 2007. **21**(9): p. 2189-202.
98. Losada, A., T. Yokochi, and T. Hirano, *Functional contribution of Pds5 to cohesin-mediated cohesion in human cells and Xenopus egg extracts.* J Cell Sci, 2005. **118**(Pt 10): p. 2133-41.

99. Geck, P., et al., *Androgen-induced proliferative quiescence in prostate cancer cells: the role of AS3 as its mediator.* Proc Natl Acad Sci U S A, 2000. **97**(18): p. 10185-90.
100. Horoszewicz, J.S., et al., *LNCaP model of human prostatic carcinoma.* Cancer Res, 1983. **43**(4): p. 1809-18.
101. Ott, H.W., et al., *Calgranulins in cystic fluid and serum from patients with ovarian carcinomas.* Cancer Res, 2003. **63**(21): p. 7507-14.
102. Cordin, O., et al., *The DEAD-box protein family of RNA helicases.* Gene, 2006. **367**: p. 17-37.
103. Sheng, Y., et al., *Gonadotropin-regulated testicular RNA helicase (GRTH/Ddx25) is a transport protein involved in gene-specific mRNA export and protein translation during spermatogenesis.* J Biol Chem, 2006. **281**(46): p. 35048-56.
104. Thomas, F.H., et al., *Thrombospondin-1 expression is increased during follicular atresia in the primate ovary.* Endocrinology, 2008. **149**(1): p. 185-92.
105. Greenaway, J., et al., *Thrombospondin-1 inhibits VEGF levels in the ovary directly by binding and internalization via the low density lipoprotein receptor-related protein-1 (LRP-1).* J Cell Physiol, 2007. **210**(3): p. 807-18.
106. Kidane, D., et al., *Kinesin 5B (KIF5B) is required for progression through female meiosis and proper chromosomal segregation in mitotic cells.* PLoS One, 2013. **8**(4): p. e58585.
107. Tian, X., G. Pascal, and P. Monget, *Evolution and functional divergence of NLRP genes in mammalian reproductive systems.* BMC Evol Biol, 2009. **9**: p. 202.
108. Wang, S., et al., *Proteome of mouse oocytes at different developmental stages.* Proc Natl Acad Sci U S A, 2010. **107**(41): p. 17639-44.
109. Yang-Hartwich, Y., et al., *p53 protein aggregation promotes platinum resistance in ovarian cancer.* Oncogene, 2015. **34**(27): p. 3605-16.
110. Yamane, T., et al., *Identification of the Critical Site of Calponin 1 for Suppression of Ovarian Cancer Properties.* Anticancer Res, 2015. **35**(11): p. 5993-9.
111. Zhu, Q., N.V. Emanuele, and D.H. Van Thiel, *Calponin is expressed by Sertoli cells within rat testes and is associated with actin-enriched cytoskeleton.* Cell Tissue Res, 2004. **316**(2): p. 243-53.
112. Rebourcet, D., et al., *Sertoli cells control peritubular myoid cell fate and support adult Leydig cell development in the prepubertal testis.* Development, 2014. **141**(10): p. 2139-49.
113. Bruney, L., et al., *Integrin-linked kinase activity modulates the pro-metastatic behavior of ovarian cancer cells.* Oncotarget, 2016. **7**(16): p. 21968-81.
114. Hennebold, J.D., et al., *Ovary-selective genes I: the generation and characterization of an ovary-selective complementary deoxyribonucleic acid library.* Endocrinology, 2000. **141**(8): p. 2725-34.
115. Matsumoto, T., et al., *Expression of ovary-specific acidic protein in steroidogenic tissues: a possible role in steroidogenesis.* Endocrinology, 2009. **150**(7): p. 3353-9.
116. Kinouchi, R., et al., *Distribution of CESP-1 protein in the corneal endothelium and other tissues.* Invest Ophthalmol Vis Sci, 2006. **47**(4): p. 1397-403.
117. Qi, S., et al., *A mitochondria-localized glutamic acid-rich protein (MGARP/OSAP) is highly expressed in retina that exhibits a large area of intrinsic disorder.* Mol Biol Rep, 2011. **38**(5): p. 2869-77.

118. Zhou, M., et al., *The expression of a mitochondria-localized glutamic acid-rich protein (MGARP/OSAP) is under the regulation of the HPG axis.* Endocrinology, 2011. **152**(6): p. 2311-20.
119. Billard, L.M., et al., *MeCP2 and MBD2 expression during normal and pathological growth of the human mammary gland.* Oncogene, 2002. **21**(17): p. 2704-12.
120. Feng, H., et al., *Identification of significant genes with poor prognosis in ovarian cancer via bioinformatical analysis.* J Ovarian Res, 2019. **12**(1): p. 35.
121. Gan, Y., et al., *Knockdown of HMGN5 increases the chemosensitivity of human urothelial bladder cancer cells to cisplatin by targeting PI3K/Akt signaling.* Oncol Lett, 2017. **14**(6): p. 6463-6470.
122. Weng, M., et al., *The high-mobility group nucleosome-binding domain 5 is highly expressed in breast cancer and promotes the proliferation and invasion of breast cancer cells.* Tumour Biol, 2015. **36**(2): p. 959-66.
123. Wang JW, Z.L., Yang XZ, Ai JK, Xin DQ, Na YQ, Guo YL. , *The NSBP1 expression is up-regulated in prostate cancer cell.* Basic Med Sci Clin., 2004. **24**: p. 393-397.
124. Jerkovic, L., et al., *Afamin is a novel human vitamin E-binding glycoprotein characterization and in vitro expression.* J Proteome Res, 2005. **4**(3): p. 889-99.
125. Dieplinger, B., et al., *Analytical characterization and clinical evaluation of an enzyme-linked immunosorbent assay for measurement of afamin in human plasma.* Clin Chim Acta, 2013. **425**: p. 236-41.
126. Koninger, A., et al., *Serum concentrations of afamin are elevated in patients with polycystic ovary syndrome.* Endocr Connect, 2014. **3**(3): p. 120-6.
127. Silva, J.M., et al., *Cyfip1 is a putative invasion suppressor in epithelial cancers.* Cell, 2009. **137**(6): p. 1047-61.
128. Yamazaki, D., T. Oikawa, and T. Takenawa, *Rac-WAVE-mediated actin reorganization is required for organization and maintenance of cell-cell adhesion.* J Cell Sci, 2007. **120**(Pt 1): p. 86-100.
129. Yamaguchi, H. and J. Condeelis, *Regulation of the actin cytoskeleton in cancer cell migration and invasion.* Biochim Biophys Acta, 2007. **1773**(5): p. 642-52.
130. Brinkmann, U., et al., *Role of CAS, a human homologue to the yeast chromosome segregation gene CSE1, in toxin and tumor necrosis factor mediated apoptosis.* Biochemistry, 1996. **35**(21): p. 6891-9.
131. Tanner, M.M., et al., *Increased copy number at 20q13 in breast cancer: defining the critical region and exclusion of candidate genes.* Cancer Res, 1994. **54**(16): p. 4257-60.
132. Isola, J.J., et al., *Genetic aberrations detected by comparative genomic hybridization predict outcome in node-negative breast cancer.* Am J Pathol, 1995. **147**(4): p. 905-11.
133. Brinkmann, U., et al., *The human CAS (cellular apoptosis susceptibility) gene mapping on chromosome 20q13 is amplified in BT474 breast cancer cells and part of aberrant chromosomes in breast and colon cancer cell lines.* Genome Res, 1996. **6**(3): p. 187-94.
134. Tirkkonen, M., et al., *Distinct somatic genetic changes associated with tumor progression in carriers of BRCA1 and BRCA2 germ-line mutations.* Cancer Res, 1997. **57**(7): p. 1222-7.

135. Peiro, G., et al., *Cellular apoptosis susceptibility gene expression in endometrial carcinoma: correlation with Bcl-2, Bax, and caspase-3 expression and outcome.* Int J Gynecol Pathol, 2001. **20**(4): p. 359-67.
136. Zhang, L., et al., *Pyridoxine 5'-phosphate oxidase is a novel therapeutic target and regulated by the TGF-beta signalling pathway in epithelial ovarian cancer.* Cell Death Dis, 2017. **8**(12): p. 3214.
137. Ames, B.N., *DNA damage from micronutrient deficiencies is likely to be a major cause of cancer.* Mutat Res, 2001. **475**(1-2): p. 7-20.
138. Yang, X., et al., *Gene variants identified by whole-exome sequencing in 33 French women with premature ovarian insufficiency.* J Assist Reprod Genet, 2019. **36**(1): p. 39-45.
139. Gabriel, M., et al., *Role of the splicing factor SRSF4 in cisplatin-induced modifications of pre-mRNA splicing and apoptosis.* BMC Cancer, 2015. **15**: p. 227.
140. Dvinge, H., et al., *RNA splicing factors as oncoproteins and tumour suppressors.* Nat Rev Cancer, 2016. **16**(7): p. 413-30.
141. Oltean, S. and D.O. Bates, *Hallmarks of alternative splicing in cancer.* Oncogene, 2014. **33**(46): p. 5311-8.
142. Ramalho, R.F. and D.M. Carraro, *Increasing evidence for the presence of alternative proteins in human tissues and cell lines.* Applied Cancer Research, 2017. **37**(1): p. 10.
143. Al-Hakim, A., et al., *The ubiquitous role of ubiquitin in the DNA damage response.* DNA Repair (Amst), 2010. **9**(12): p. 1229-40.
144. Dianov, G.L., C. Meisenberg, and J.L. Parsons, *Regulation of DNA repair by ubiquitylation.* Biochemistry (Moscow), 2011. **76**(1): p. 69-79.
145. Ajuh, P., et al., *Functional analysis of the human CDC5L complex and identification of its components by mass spectrometry.* Embo j, 2000. **19**(23): p. 6569-81.
146. Zhang, N., et al., *Cdc5L interacts with ATR and is required for the S-phase cell-cycle checkpoint.* EMBO Rep, 2009. **10**(9): p. 1029-35.
147. Liu, X.M., et al., *Single-cell transcriptome sequencing reveals that cell division cycle 5-like protein is essential for porcine oocyte maturation.* J Biol Chem, 2018. **293**(5): p. 1767-1780.
148. Malinova, A., et al., *Assembly of the U5 snRNP component PRPF8 is controlled by the HSP90/R2TP chaperones.* J Cell Biol, 2017. **216**(6): p. 1579-1596.
149. Small, E.C., et al., *The EF-G-like GTPase Snu114p regulates spliceosome dynamics mediated by Brr2p, a DExD/H box ATPase.* Mol Cell, 2006. **23**(3): p. 389-99.
150. Marzano, V., et al., *Proteomic profiling of ATM kinase proficient and deficient cell lines upon blockage of proteasome activity.* J Proteomics, 2012. **75**(15): p. 4632-46.

**Figure 1**

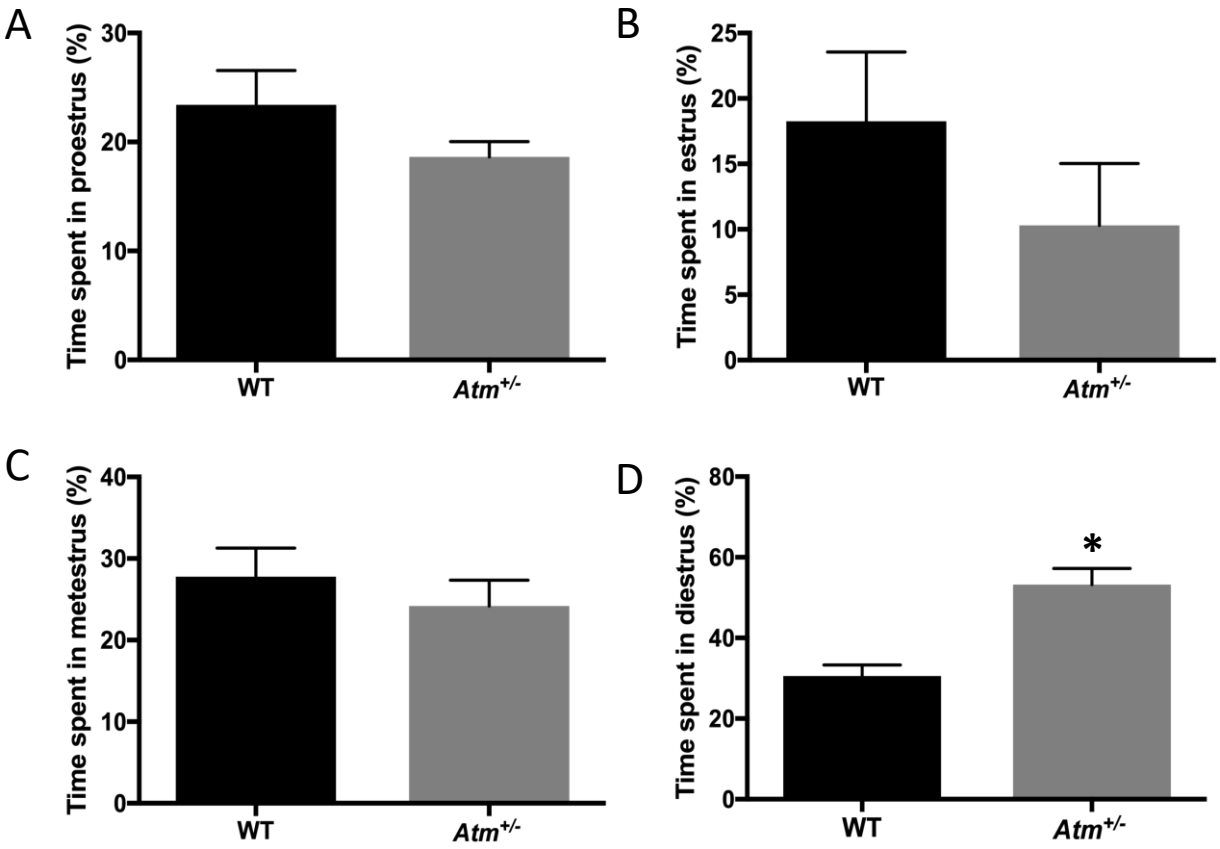

**Figure 2**

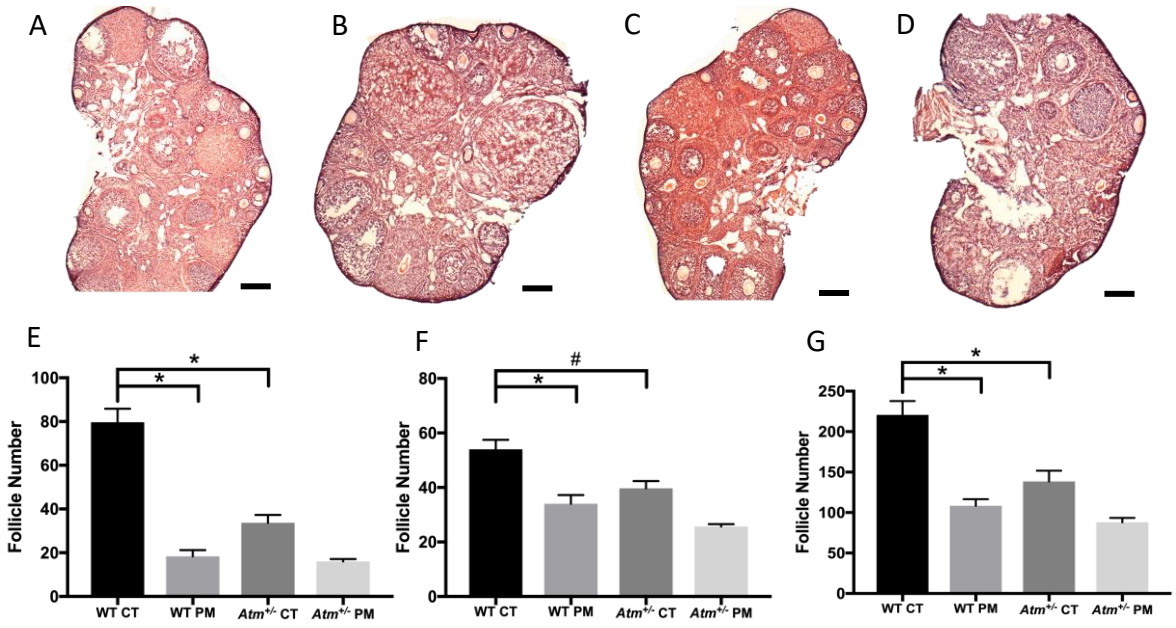

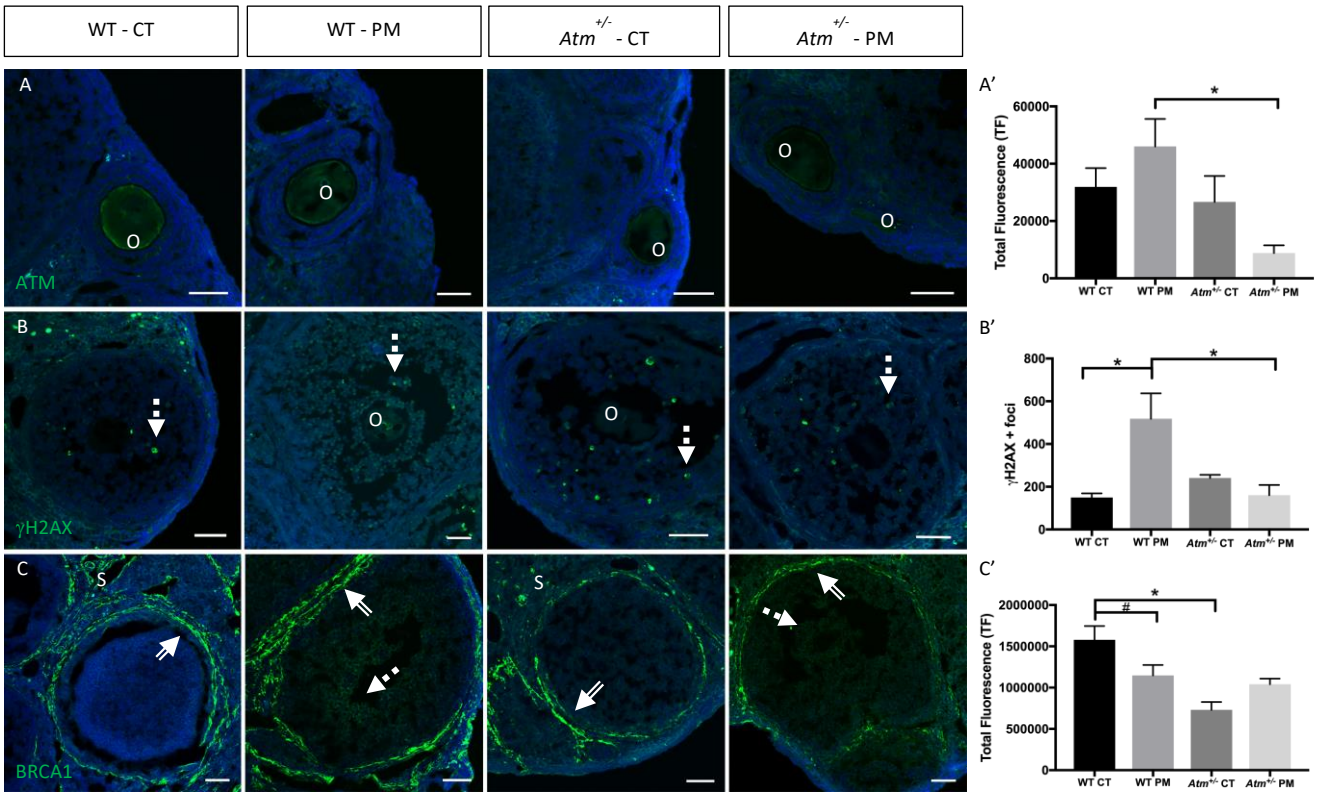

**Figure 4**

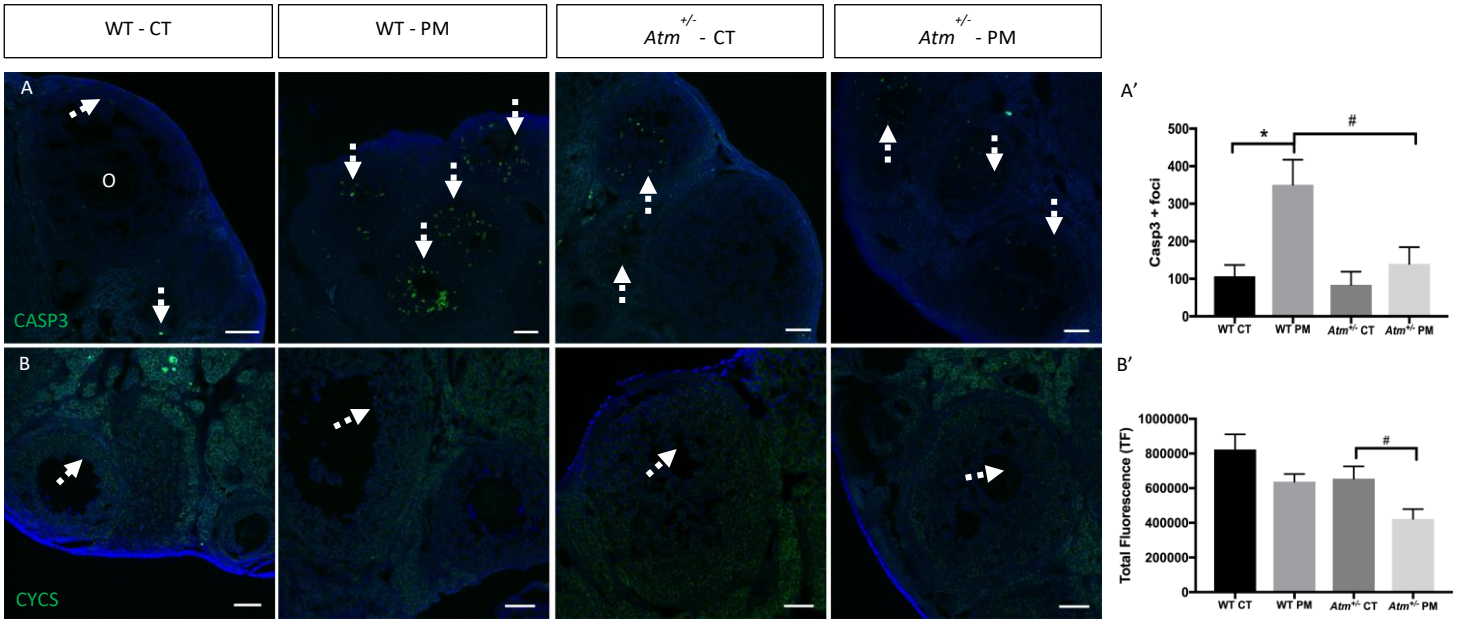

# Figure 5

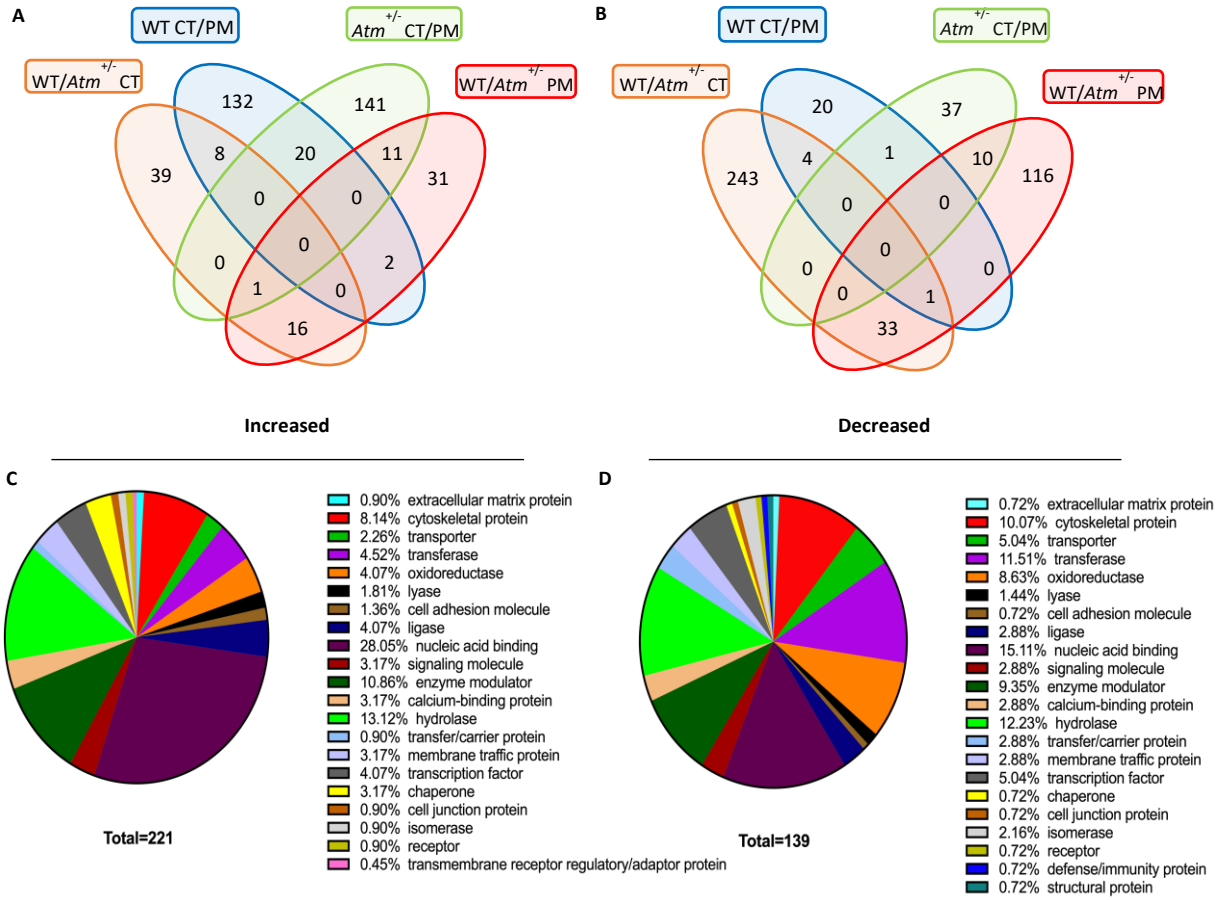

**Figure 6**